PERGAMON

International Journal of Multiphase Flow 28 (2002) 1589–1616

International Journal of Multiphase Flow

www.elsevier.com/locate/ijmulflow

Two-phase laminar flow in a heated microchannels

L.P. Yarin, L.A. Ekelchik, G. Hetsroni *

Department of Mechanical Engineering, Technion—Israel Institute of Technology, 32000 Haifa, Israel

Received 15 September 2001; received in revised form 18 June 2002

Abstract

This paper deals with the theory of two-phase laminar flow in a heated microchannels. The main objective of the work is to study the thermohydrodynamic characteristics of a two-phase capillary flow with phase change at the meniscus. A quasi-one-dimensional model is proposed for such a flow. It takes into account the principal characteristics of the phenomenon, namely, the effects of the inertia, pressure, gravity, friction forces and capillary pressure due to the curvature of the interface surface, as well as the thermal and dynamical interactions of the liquid and vapor phases. To describe the flow outside of the meniscus, in the domains of the pure liquid or vapor, the one-dimensional mass, momentum and energy equations are used. The possible states of the flow are considered, and the domains of steady and unsteady states are outlined. An equation for stationary two-phase flow regimes in heated microchannel is derived. This equation is applied to classify the operating parameters, corresponding to various types of flow.

1. Introduction

One possible way to enhance heat transfer in cooling systems of electronic devices, with high power densities, is phase change of the coolant in microchannels. The possibility enchance heat transfer motivated a number of studies of two-phase boiling heat transfer in mini- and microchannels (Bowers and Mudawar, 1994; Morijama and Inoue, 1992; Landerman, 1994; Peng et al., 1996; Peng and Wang, 1998).

Two-phase flows in the microchannels with an evaporating meniscus, which separates the regions of liquid and vapor, have been considered by Khrustalev and Faghri (1995) and Peles et al. (1998, 2000). In the latter a quasi-one-dimensional model was used to analyze the thermohydrodynamic characteristics of the flow in a heated capillary, with a distinct interface. This model

* Corresponding author. Tel.: +972-4-829-2058; fax: +972-4-832-4533.
E-mail address: hetsroni@tx.technion.ac.il (G. Hetsroni).

0301-9322/02/$ - see front matter
PII: S0301-9322(02)00050-2

takes into account the multistage character of the process, as well as the effect of capillary, friction and gravity forces on the flow development. The theoretical and experimental studies of the steady forced flow in a microchannel with evaporating meniscus were recently carried out by Peles et al. (2001). These studies reveal the effect of a number of dimensionless parameters such as the Peclet and Jakob numbers, dimensionless heat transfer flux, etc. on the velocity, temperature and pressure distributions in the liquid and vapor regions. The structure of flow in heated microchannel is determined by number of factors: the physical properties of fluid, its velocity, heat flux on the wall, etc. At a fixed geometry, the flow pattern in microchannel depends, mainly, on the liquid velocity v and heat flux on the wall q_w (i.e. the values of the Peclet number and dimensionless heat flux) different regimes of flow take place. At large q_w and small v the bubbles nucleation is the dominant factor that determines the flow pattern. In the case of relatively small q_w and large v the bubbles nucluation is negligible. Under these conditions two-phase flow with distinct meniscus which divides the region of pure liquid and pure vapor flows forms in microchannel. Such flow characterize small channels with high critical heat flux.

In spite of the fact that for the last decade the flow in microchannels has attracted significant interest (Incropera, 1999; Peng and Wang, 1994; Peng et al., 1994; Ha and Peterson, 1998; Peterson and Ha, 1998; Triplett et al., (Part I) 1999; Triplett et al., (Part II) 1999; Ghiaasiaan and Abdel-Khalik, 2001) a number of important problems related to the hydrodynamic and heat transfer in such channels, were less investigated. This particularly concerns the parametrical dependence of the process, its stability, conditions of the existence of stationary flow, etc.

The main goal of the present work is to study the complex processes in heated microchannels with evaporating meniscus. The study consists of the formulation of the problem, detailed analysis of the influence of the physical properties of the coolant and wall heat flux on the thermal regime of the flow, hydraulic resistance of the microchannel, as well as the efficiency of the cooling system in the whole.

The model of the cooling system of electronic device with high power density is described in Section 2. Section 3 deals with the mathematical formulation of the problem of laminar flow in a heated capillary with phase change. The statement of the dimensionless variables, re-formulation of the problem in these variables, its parametrical study, as well as the analysis of the existence of steady and unsteady states are presented in Sections 4–6. In Section 7 we discuss the results of the numerical calculations. The problem of efficiency of the cooling system and the condition of its optimal functioning are presented in Section 8. The relation between the saturation parameters of the vapor are presented in Appendix A. The integral relations are derived in Appendix B. The analysis of the solutions of the governing system of equations is presented in Appendix C.

2. Model of cooling system

The elements of a cooling system of electronic devices are micro-heat-exchangers with extremely large surface area per unit volume, low thermal resistance and small mass. As a rule, they are a system of parallel channels with hydraulic diameters from 10 to 10^3 μm with inlet and outlet manifolds, which connect the channels (Fig. 1). A sketch of the cooling system of an electronic device is presented in Fig. 2. It consists of a microchannel (1), condenser (2), heat exchanger (3), pump (4) and tanks (5) and (6). The coolant is supplied into the microchannel (by the pump),

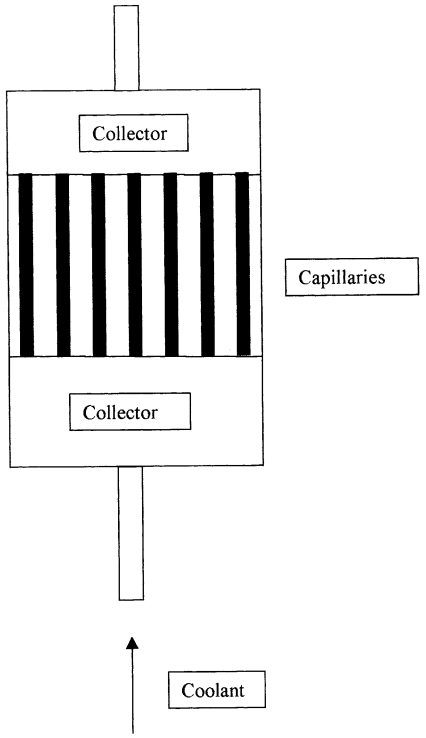

Fig. 1. Cooling element of electronic device.

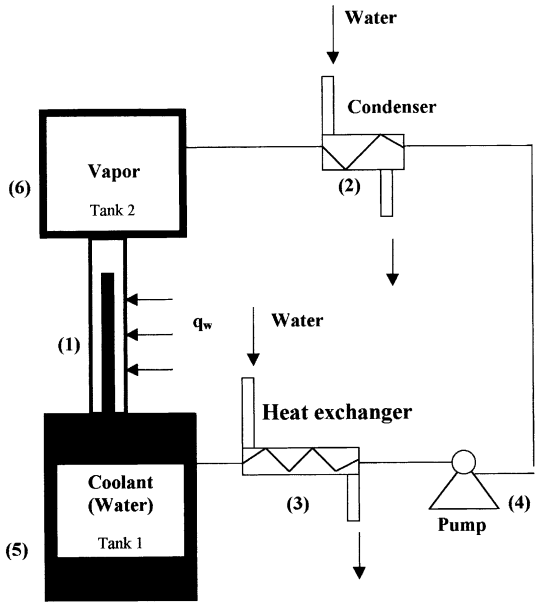

Fig. 2. Scheme of a cooling system.

where it is heated and vaporizes on the meniscus. The vapor enters into the vapor tank (6) and then into the condenser (2) where it condenses. The water from the condenser (2) enters into the heat exchanger (3) and is cooled down to ambient temperature. The pressure $P_{2.0}$ and temperature $T_{2.0}$ at the inlet of the microchannel can be changed by regulating the heat exchanger and the pump.

The thermohydrodynamic characteristics of the flow in the heated microchannels depend on the following factors: the heat flux on the wall, which determines the intensity of the vaporization, the location of the meniscus, the difference between the inlet and outlet pressures, the capillary, mass and friction forces which act on the liquid and the vapor.

The processes in a cooling system of electronic devices with high power density can be modeled as follows. The coolant with temperature $T_{2.0}$ and pressure $P_{2.0}$ enters into the microchannel from the tank (5) (Fig. 2). The mass capacity of the liquid in the tank (5) is large enough, therefore the heat flux from the microchannel does not influence the coolant initial temperature. Phase change occurs directly on the meniscus. Its position depends on the operating parameters and the physical properties of the cooling fluid and its vapor. The upper tank (6) and the condenser (2) ensure a given pressure of the vapor at the outlet of the microchannel.

3. Formulation of the problem

3.1. Conditions on the interfacial surface

The existence of the interfacial surface with a finite curvature causes the capillary pressure, which determines the rising of the liquid, and its height in a stationary state (Levich, 1962). The latter is determined by the equilibrium of the gravity and capillary forces. The situation changes drastically, when the phase change occurs on the meniscus surface. The liquid evaporation provides for the motion of both phases and displacement of the interface. In this case the flow field is demarcated by the interface into two domains where pure liquid or vapor flow occurs. Obviously, that such structure of flow in microchannel is possible, when bubble nucleation within the liquid domain is absent. The theoretical analysis by Peng et al. (1998) showed, that the critical value of the heat flux on the wall at which the bubble nucleation is negligible depends on the physical properties of the liquid, the microchannel diameter and is expressed by the following inequality:

$$\frac{q_e \alpha}{c\pi(v'' - v')d} > q_{cr}, \tag{1}$$

where q_e is the latent heat of evaporation, v'' and v' are the vapor and liquid specific volume at saturation, α is the thermal diffusivity of the vapor, d is the microchannel diameter, c is an empirical constant has order of unity. For water flow in microchannel $d = 10^{-4}$ m ($v'' = 1.673$ m^3/kg, $v' = 0.00104$ m^3/kg, $q_e = 2.26 \times 10^6$ J/kg, $\alpha = 18.58 \times 10^{-8}$ m^2/s) critical heat flux q_{cr} is about 8×10^4 W/m^2 and increases with d decreasing. In experiments by Peng and Wang (1993), Peng et al. (1994, 1996) vapor bubbles were not observed in water and methanol flows in rectangular microchannels with cross-section ranging from 0.1×0.3 to 0.6×0.7 mm even when the applied heat flux was much higher than 10^5 W/m^2. Thus, the theoretical estimations, as well as experiment

show that the considered model of flow in heated microchannel is valid for highly wide range of heat fluxes, which are of practical interest.

Consider a flow of liquid coolant in a capillary where heating and evaporation occur. The conditions on the interface are expressed by means of the equations continuity of the mass and thermal fluxes and the equilibrium of all acting forces (Landau and Lifshiz, 1959):

$$\sum_{i=1}^{2}(\rho_i \mathbf{v}_i)\cdot \mathbf{n}_i = 0 \tag{2}$$

$$\sum_{i=1}^{2}(\rho_i \mathbf{v}_i h_i + \lambda_i \nabla T_i)\cdot \mathbf{n}_i = 0 \tag{3}$$

$$\sum_{i=1}^{2}(P_i + \rho_i v_{\mathrm{in}} v_{\mathrm{in}})\mathbf{n}_i = (\sigma_{*2} - \sigma_{*1})\mathbf{k} + \sigma(r_1^{-1} + r_2^{-1})\mathbf{n}_2 + \nabla\sigma \tag{4}$$

where ρ, $\mathbf{v}$, T, h and P are the density, velocity, temperature, enthalpy and pressure; σ is the surface tension; λ is the thermal conductivity; σ_* is the viscous tension tensor; $v_{\mathrm{in}} = \mathbf{v}_i \cdot \mathbf{n}_i$ and $\nabla T_i \cdot \mathbf{n}_i$ are the normal components of the velocity vector and the interface surface temperature gradient, respectively; r_1 and r_2 are the general radii of the curvature for the interface; $\mathbf{n}$ and $\mathbf{k}$ are the normal and tangent directions; $\mathbf{n}_1 = -\mathbf{n}_2$; $i = 1, 2$ refer to the vapor and the liquid; the bold letters means the vector.

Consider a system liquid/solid for which the contact angle is close to 90° (for example, the contact angle for the system water/steel is $70° < \theta < 90°$, (Grigoriev and Zorin, 1982). The projections of the velocity vector $\mathbf{v}$ on x, y, z-axes are $u = |\mathbf{v}|\sin\theta$, $v = w = |\mathbf{v}|\cos\theta$. Since for the surface, which is bent weakly, $\cos\theta \ll 1$ and $\sin\theta \sim 1$ we have the following estimate $u \gg v = w$. Analogously, $\partial T/\partial x \gg \partial T/\partial y = \partial T/\partial z$.

Bearing in mind these estimates and the assumptions that $\sigma = \text{const.}$ and the fluid is incompressible, Eqs. (2)–(4) transform as follows:

$$\rho_1 \widetilde{V}_1 = \rho_2 \widetilde{V}_2 \tag{5}$$

$$P_1 + \rho_1 \widetilde{V}_1^2 = P_2 + \rho_2 \widetilde{V}_2^2 + f_{\mathrm{L}} \tag{6}$$

$$\rho_1 \widetilde{V}_1 h_1 - \lambda_1 \frac{\partial T_1}{\partial x} = \rho_2 \widetilde{V}_2 h_2 - \lambda_2 \frac{\partial T_2}{\partial x} \tag{7}$$

where $\widetilde{V}_i = u_i - V_{\mathrm{f}}$ is the relative velocity, $V_{\mathrm{f}} = \partial x_{\mathrm{f}}/\partial t$ is the velocity of interface surface, $f_{\mathrm{L}} = 2\sigma/R$ is the capillary pressure, $R = r_1 = r_2$ is the radius of the surface curvature.

Since the coolant and its vapor are conductive fluids, $T_{1.\mathrm{f}} = T_{2.\mathrm{f}} = T_{\mathrm{s}}$, where the subscripts s and f correspond to the saturation parameters and the interface surface. The saturation pressure and temperature are connected weakly (Appendix A), so that T_{s} is determined practically by the external pressure $P_{1.00}$.

It should be stressed, that Eqs. (5) and (6) are satisfied for any values of the contact angle, whereas Eq. (7) is correct only for θ that is close to 90°.

3.2. The flow outside of the interfacial surface

To calculate the flow fields outside of the evaporating meniscus we use the one-dimensional model, developed by Peles et al. (1998, 2000, 2001). Assuming that the compressibility and the energy dissipation are negligible (a flow with moderate velocities), the thermal conductivity and viscosity are independent of the pressure and temperature, we arrive at the following system of equations:

$$\frac{\partial \rho_i}{\partial t} + \frac{\partial \rho_i u_i}{\partial x} = 0 \tag{8}$$

$$\rho_i \frac{\partial u_i}{\partial t} + \rho_i u_i \frac{\partial u_i}{\partial x} = -\frac{\partial P_i}{\partial x} - \rho_i g - \frac{\partial F_i}{\partial x} \tag{9}$$

$$\rho_i \frac{\partial h_i}{\partial t} + \rho_i u_i \frac{\partial h_i}{\partial x} = \frac{\partial}{\partial x}\left(\lambda_i \frac{\partial T_i}{\partial x}\right) + q, \tag{10}$$

where F is the specific friction force, q is the specific volumetric rate of heat absorption, g is the acceleration due to gravity.

The initial and boundary conditions for the problem are

$$t = 0 : \rho_i = \rho_i(x), \quad u_i = u_i(x), \quad T_i = T_i(x), \quad h_i = h_i(x), \quad x_\mathrm{f} = x_\mathrm{f}^*, \tag{11}$$

where the x is the longitudinal coordinate; x_f and x_f^* are the meniscus actual and initial position.

$$t > 0 : x = 0, \quad \rho_2 = \rho_{2.0}, \quad u_2 = u_{2.0}, \quad T_2 = T_{2.0}, \quad h_2 = h_{2.0}, \quad P_2 = P_{2.0} \tag{12}$$

$$t > 0 : x = x_\mathrm{f}^*, \quad \rho_i = \rho_{\mathrm{i.f}}, \quad u_i = u_{\mathrm{i.f}}, \quad T_i = T_{\mathrm{i.f}}, \quad h_i = h_{\mathrm{i.f}}, \quad P_i = P_{\mathrm{i.f}} \tag{13}$$

$$t > 0 : x = L, \quad \rho_1 = \rho_{1.00}, \quad u_1 = u_{1.00}, \quad \frac{\partial T_1}{\partial x} = 0, \quad \frac{\partial h_1}{\partial x} = 0, \quad P_1 = P_{1.00} \tag{14}$$

where L is the total length of the microchannel, subscripts 0 and 00 are related to the inlet and outlet, respectively (Fig. 3).

The boundary conditions (12)–(14) correspond to the flow in a microchannel with a cooled inlet and adiabatic reciever (an adiabatic pipe or tank, which is established at the exit of the microchannel). Note, that the boundary conditions of the problem can be formulated by another way, if the cooling system has another construction, for example, as follows: $x = 0$, $T_2 = T_{2.0}$, $x = L$, $T_1 = T_{1.00}$, when the inlet and outlet are cooled; $x = 0$, $\partial T_2/\partial x = 0$, $x = L$, $T_1 = T_{1.00}$ in case of the adiabatic inlet and the cooled outlet, etc.

We supplement the system of Eqs. (8)–(10) by the equations of state of the vapor and liquid

$$P_1 = \rho_1 R T_1 \tag{15}$$

$$\rho_2 = \rho_2(T_2), \tag{16}$$

and by the equation for the vapor pressure at the interface surface.

$$P_{1.\mathrm{f}} = P_{1.\mathrm{f}}(T_{1.\mathrm{f}}) \tag{17}$$

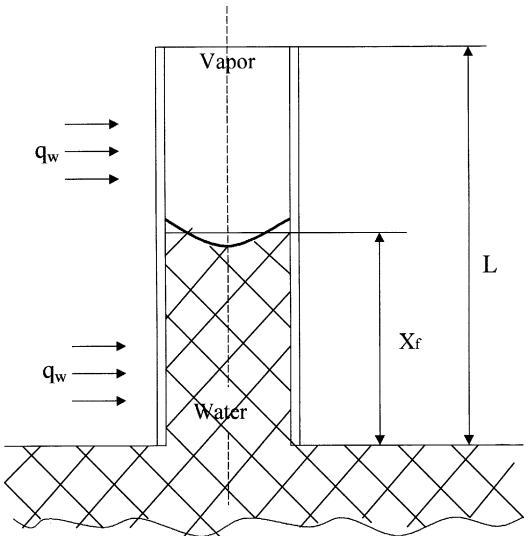

Fig. 3. Characteristic domains in heated capillary: (a) flow of vapor, (b) flow of liquid (hold line is interphase).

The quasi-one-dimensional model is based on the system of Eqs. (8)–(10) with condition (5)–(7) and describes the major features of the flow in the heated capillary. This model takes into account the general characteristics of the process due to the curvature of the interfacial surface, as well as the flow of the liquid and vapor, that is caused by evaporation. Similar model was successfully used by Yuan and Prosperetti (1999) for a study on the pumping effect of growing and collapsing bubbles in a tube. It should be noted that the actual position of the meniscus x_f, as well as the velocity of the coolant at the inlet $u_{2.0}$, and the vapor temperature at the outlet of the micro-channel $T_{1.00}$ are a priori unknown. In order to determine these parameters it is necessary to supply the system of governing equations, the integral correlations connecting inlet and outlet parameters. They take the following form (Appendix B):

$$\frac{\partial}{\partial t}\left(\int_0^{x_f}\rho_2\,dx+\int_{x_f}^{L}\rho_1\,dx\right)+(\rho_{1.00}u_{1.00}-\rho_{2.0}u_{2.0})=0 \tag{18}$$

$$\frac{\partial}{\partial t}\left(\int_0^{x_f}\rho_2u_2\,dx+\int_{x_f}^{L}\rho_1u_1\,dx\right)=f_L-\left\{(\rho_1u_1^2)_{00}-(\rho_2u_2^2)_0\right\}+(P_{2.0}-P_{1.00})-g\left(\int_0^{x_f}\rho_2\,dx+\int_{x_f}^{L}\rho_1\,dx\right)-(F_{2.f}+F_{1.00}) \tag{19}$$

$$\frac{\partial}{\partial t}\left(\int_0^{x_f}\rho_2h_2\,dx+\int_{x_f}^{L}\rho_1h_1\,dx\right)+\left\{(\rho_1u_1h_1)_{00}-(\rho_2u_2h_2)_0\right\}=-\lambda_2\left(\frac{\partial T_2}{\partial x}\right)_0+qL \tag{20}$$

Note, that the term $\lambda_1(\partial T_1/\partial x)_{00}$ which belongs to the boundary condition (14) is omitted on the r.h.s. of Eq. (20).

4. Non-dimensional variables

Assuming steady state in Eqs. (8)–(10) and (18)–(20), we obtain the system of equations which determines steady regimes of the flow in the heated microchannel. Introduce values of density $\rho_* = \rho_{2.0}$, velocity u_*, length $l_* = L$, temperature $T_* = T_{2.0}$, pressure $\Delta P_* = P_{2.0} - P_{1.00}$ and enthalpy q_e as characteristic scales. Define the dimensionless variables as follows:

$$\bar{\rho} = \rho/\rho_*, \quad \bar{u} = u/u_*, \quad \bar{x} = x/l_*, \quad \overline{T} = T/T_*,$$
$$\bar{h} = h/q_e, \quad \gamma = \frac{\lambda T_*}{\rho_* u_* q_e l_*}, \quad \overline{P} = P/\Delta P_* \tag{21}$$

we obtain the dimensionless equations

$$\frac{d\bar{\rho}_i \bar{u}_i}{d\bar{x}} = 0 \tag{22}$$

$$\bar{\rho}_i \bar{u}_i \frac{d\bar{u}_i}{d\bar{x}} = -Eu \frac{d\overline{P}_i}{d\bar{x}} - Fr^{-1}\bar{\rho}_i - \frac{d\overline{F}_i}{d\bar{x}} \tag{23}$$

$$\bar{\rho}_i \bar{u}_i \frac{d\bar{h}_i}{d\bar{x}} = \gamma_i \frac{d^2\overline{T}_i}{d\bar{x}^2} + \vartheta, \tag{24}$$

where $Eu = \Delta P_*/\rho_* u_*^2$ and $Fr = u_*^2/gL$ are the Euler and Froude numbers, $\vartheta = qL/\rho_* u_* q_e$, $\overline{F}_i = F_i/\rho_* u_*^2$, $\gamma_i = \tilde{q}_i/Pe_i$, $\tilde{q}_i = c_{pi} T_*/q_e$, $Pe_i = u_* L/\alpha_i$ is the Peclet number, $\alpha_i = \lambda_i/\rho_* c_{pi}$.

Choose the characteristic velocity u_* so, that total heat flux on the wall is fully used for liquid evaporation (the heating without any losses of heat: $\vartheta \equiv 1$). We conclude that

$$u_* = \frac{qL}{\rho_* q_e} = \frac{4 q_w L}{d \rho_* q_e}, \tag{25}$$

The conditions (5)–(7) and integral relations (18)–(20) become

$$\bar{\rho}_1 \overline{\overline{V}}_1 = \bar{\rho}_2 \overline{\overline{V}}_2 \tag{26}$$

$$Eu\overline{P}_1 + \bar{\rho}_1 (\overline{\overline{V}}_1)^2 = Eu\overline{P}_2 + \bar{\rho}_2 (\overline{\overline{V}}_2)^2 + We^{-1} \tag{27}$$

$$\bar{\rho}_1 \overline{\overline{V}}_1 \bar{h}_1 - \gamma_1 \frac{\partial \overline{T}_1}{\partial \bar{x}} = \bar{\rho}_2 \overline{\overline{V}}_2 \bar{h}_2 - \gamma_2 \frac{\partial \overline{T}_2}{\partial \bar{x}} \tag{28}$$

and

$$\bar{\rho}_{1.00} \bar{u}_{1.00} - \bar{\rho}_{2.0} \bar{u}_{2.0} = 0 \tag{29}$$

$$We^{-1} - \left\{ (\bar{\rho}_1 \bar{u}_1^2)_{00} - (\bar{\rho}_2 \bar{u}_2^2)_0 \right\} + Eu - Fr^{-1} \left(\int_0^{\bar{x}_f} \bar{\rho}_2 \, d\bar{x} + \int_{\bar{x}_f}^{\overline{L}} \bar{\rho}_1 \, d\bar{x} \right) - (\overline{F}_{2.f} + \overline{F}_{1.00}) = 0 \tag{30}$$

$$(\bar{\rho}_1 \bar{u}_1 \bar{h}_1)_{00} - (\bar{\rho}_2 \bar{u}_2 \bar{h}_2)_0 = -\gamma_2 \left(\frac{\partial \overline{T}_2}{\partial \bar{x}} \right)_0 + 1, \tag{31}$$

where $We = \rho_* u_*^2 2R/\sigma$ is the Weber number, $R = d/2\cos\theta$, d is the diameter of microchannel.

The system of Eqs. (22)–(24) and relations (26)–(31) contains five dimensionless parametrical groups Eu, Fr, We, γ_1 and γ_2, which completely determine the problem.

5. Parametrical equation

Now let us transform the integral relations (30) and (31). For this, we write the solution of Eqs. (22) and (24). They are (Peles et al., 2001)

$$\bar{\rho}_i \bar{u}_i = \text{const.} \tag{32}$$

$$\overline{T}_2 = C_1^{(2)} + \vartheta^* [\bar{x} + (Pe\,\bar{u}_{2.0})^{-1}] + C_2^{(2)} \exp(Pe\,\bar{x}\bar{u}_{2.0}) \tag{33}$$

where

$$C_1^{(2)} = (1 - C_2^{(2)}) - \frac{\vartheta^*}{Pe\,\bar{u}_{2.0}}, \quad C_2^{(2)} = \frac{(\overline{T}_s - 1) - \vartheta^* \bar{x}_f}{\exp(Pe\,\bar{x}_f \bar{u}_{2.0}) - 1}, \quad \vartheta^* = \frac{q_e}{c_p T_* \bar{u}_{2.0}},$$

$\overline{T}_s = T_s/T_*$, T_s is the temperature on the interface.

We also determine the friction forces $F_{2.f}$ and $F_{1.00}$. Assume that

$$F_i = \int_{x_i'}^{x_i''} \eta_i \frac{\rho_i u_i^2}{2} \frac{dx}{d} \tag{34}$$

and take into account that $x_2' = 0$, $x_2'' = x_f$, $x_1' = x_f$, $x_1'' = L$ and $\eta_i = 64/Re_i$ ($Re_i = u_i d/v_i$, where v_i are the kinematic viscosity) we obtain

$$F_{2.f} = \frac{8}{r^2} u_2 \mu_2 x_f \tag{35}$$

$$F_{1.00} = \frac{8}{r^2} u_1 \mu_1 (L - x_f), \tag{36}$$

where r is the microchannel radius and μ is the dynamic viscosity of the fluid.

Then the last term in l.h.s. of Eq. (30) turns out to be

$$(\overline{F}_{2.f} + \overline{F}_{1.00}) = \frac{32}{Re_2} \bar{u}_2 [\bar{x}_f + v_{12}(\overline{L} - \bar{x}_f)] \widetilde{L} \tag{37}$$

where $Re_2 = u_* d/v_2$, $v_{1.2} = v_1/v_2$, $\widetilde{L} = L/d$.

Since $\bar{\rho}_1 \bar{u}_1 = \bar{\rho}_2 \bar{u}_2$, the l.h.s. of Eq. (31) is

$$(\bar{\rho}_1 \bar{u}_1 \bar{h}_1)_{00} - (\bar{\rho}_2 \bar{u}_2 \bar{h}_2)_0 = \bar{\rho}_2 \bar{u}_2 (\bar{h}_{1.00} - \bar{h}_{2.0}) \tag{38}$$

R.h.s. of Eq. (38) transforms to

$$\bar{\rho}_2 \bar{u}_2 (\bar{h}_{1.00} - \bar{h}_{2.0}) = \bar{\rho}_2 \bar{u}_2 (1 + J_1 + J_2), \tag{39}$$

where $J_1 = (h_{1.00} - h_{1.f})/q_e$, $J_2 = (h_{2.f} - h_{2.0})/q_e$

Taking into account that at $P = 10^5$ N/m^2, $h_{2.f} = 417.46$ kJ/kg, $h_{1.f} = 2675$ kJ/kg and $q_e = 2258$ kJ/kg (Johnson, 1998), we obtain the following estimates for J_1 and J_2 : $0 < J_1 < 0.02$, $0 < J_2 < 0.04$ when 100 °C $< T_1 <$ 120 °C and 80 °C $< T_2 <$ 100 °C, respectively. This allows one to assume that $\bar{\rho}_2 \bar{u}_2 (1 + J_1 + J_2) \approx \bar{\rho}_2 \bar{u}_2$.

The integrals $\int_{\bar{x}_f}^{\overline{L}} \bar{\rho}_1 \, d\bar{x}$ and $\int_0^{\bar{x}_f} \bar{\rho}_2 \, d\bar{x}$ in Eq. (30) have the order of magnitudes

$$\int_{\bar{x}_f}^{\overline{L}} \bar{\rho}_1 \, d\bar{x} \sim (\overline{L} - \bar{x}_f) \bar{\rho}_1 \tag{40}$$

$$\int_0^{\bar{x}_f} \bar{\rho}_2 \, d\bar{x} \sim \bar{x}_f \bar{\rho}_2 \tag{41}$$

Since the liquid and vapor densities are estimated as $\bar{\rho}_2 \sim 1$, $\bar{\rho}_1 \sim 10^{-3}$, we have the following estimate for the ratio of the integrals (41) and (40):

$$\frac{\int_0^{\bar{x}_f} \bar{\rho}_2 \, d\bar{x}}{\int_{\bar{x}_f}^{\overline{L}} \bar{\rho}_1 \, d\bar{x}} \sim \frac{\bar{x}_f \bar{\rho}_2}{(\overline{L} - \bar{x}_f)\bar{\rho}_1} \tag{42}$$

when $\bar{x}_f \bar{\rho}_2 / ((\overline{L} - \bar{x}_f)\bar{\rho}_1) \gg 1$ the integral (40) is much smaller then the integral (41) and it can be neglected. This inequality is fulfilled for the majority of physically realistic conditions when $\bar{x}_f \gg \overline{L} \times 10^{-3}$.

Taking into account the above estimates we write Eq. (30) in the following form:

$$\bar{u}_2' = \frac{We^{-1} + Eu - Fr^{-1}\bar{x}_f}{(32/Re_2)\widetilde{L}[\bar{x}_f + v_{12}(\overline{L} - \bar{x}_f)]} \tag{43}$$

where $\bar{u}_2'$ is the velocity, defined by the momentum equation.

When the heat flux on the wall $q_w = 0$, the velocity of the fluid also equals zero. Assuming in Eq. (43) $\bar{u}_2' = 0$, we find the height of the liquid in the microchannel with no heat transfer:

$$\overline{X}_{fcap} = \frac{We^{-1} + Eu}{Fr^{-1}} \tag{44}$$

In particular, when $Eu = 0$ (pure capillary height)

$$\overline{X}_{fcap} = \frac{Fr}{We} \tag{45}$$

Using Eq. (44), we write Eq. (43) as

$$\bar{u}_2' = A \frac{1 - \tilde{x}_f}{B - \tilde{x}_f}, \tag{46}$$

where $A = Re/(32Fr\overline{L}(v_{12} - 1))$, $B = \tilde{l}(v_{12}/(v_{12} - 1))$, $\tilde{x}_f = \bar{x}_f / \overline{X}_{fcap}$, $\tilde{l} = \overline{L}/\overline{X}_{fcap}$.

As can be seen from Eq. (46) the physical realistic values of the liquid velocity $\bar{u}_2' \geqslant 0$ correspond to the confined range of the meniscus position $\tilde{x}_f : 0 < \tilde{x}_f \leqslant 1$. The existence of the upper limit in this inequality may be explained as follows: the heat flux on the wall causes liquid evaporation and determines the displacement of the meniscus. If the heat flux increases, the rate of evaporation also increases. The velocities of the flow of the two phases grow and the interface surface moves towards the inlet of the microchannel. Thus, the height of the meniscus when $q_w = 0$ is maximum and is equal to $\overline{X}_{fcap}$. Accordingly the dimensionless meniscus height $\tilde{x}_f = x_f / \overline{X}_{fcap} < 1$ for any value of the heat flux.

The dependence of $\bar{u}_2'(\tilde{x}_f)$ on different values of the parameter B is plotted in Fig. 4(a) (Appendix C, Fig. 5(a)–(c).

Taking into account Eq. (33), we transform Eq. (31) to

$$\bar{u}_2'' = 1 - \left\{ \frac{1}{Pe\,\bar{u}_2''} + \frac{\bar{q}_2(\overline{T}_s - 1)\bar{u}_2'' - \overline{X}_{fcap}\tilde{x}_f}{\exp(Pe\,\overline{X}_{fcap}\tilde{x}_f\bar{u}_2'') - 1} \right\}, \tag{47}$$

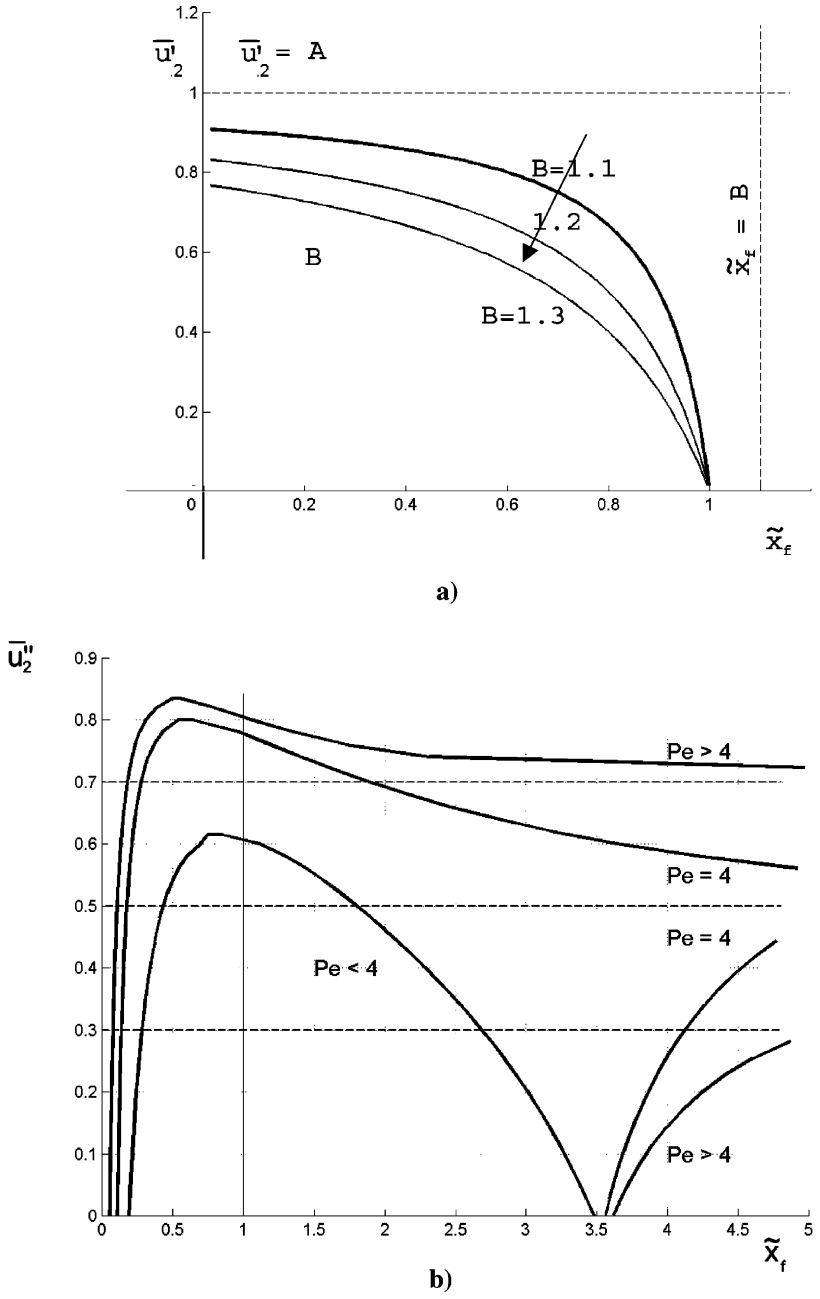

Fig. 4. Functions $\bar{u}'_2(\tilde{x}_f)$ and $\bar{u}''_2(\tilde{x}_f)$: (a) dependence of $\bar{u}'_2(\tilde{x}_f)$ upon various values of parameter B; arrow shows an increase of parameter B, (b) dependence of $\bar{u}''_2(\tilde{x}_f)$ upon various values of Peclet number.

where $\bar{u}''_2$ is the liquid velocity defined from the energy equation, $\bar{q}_2 = c_{p2}T_*/q_e$. The graphs of $\bar{u}''_2(\tilde{x}_f)$ for different values of the Peclet number are plotted in Fig. 4(b).

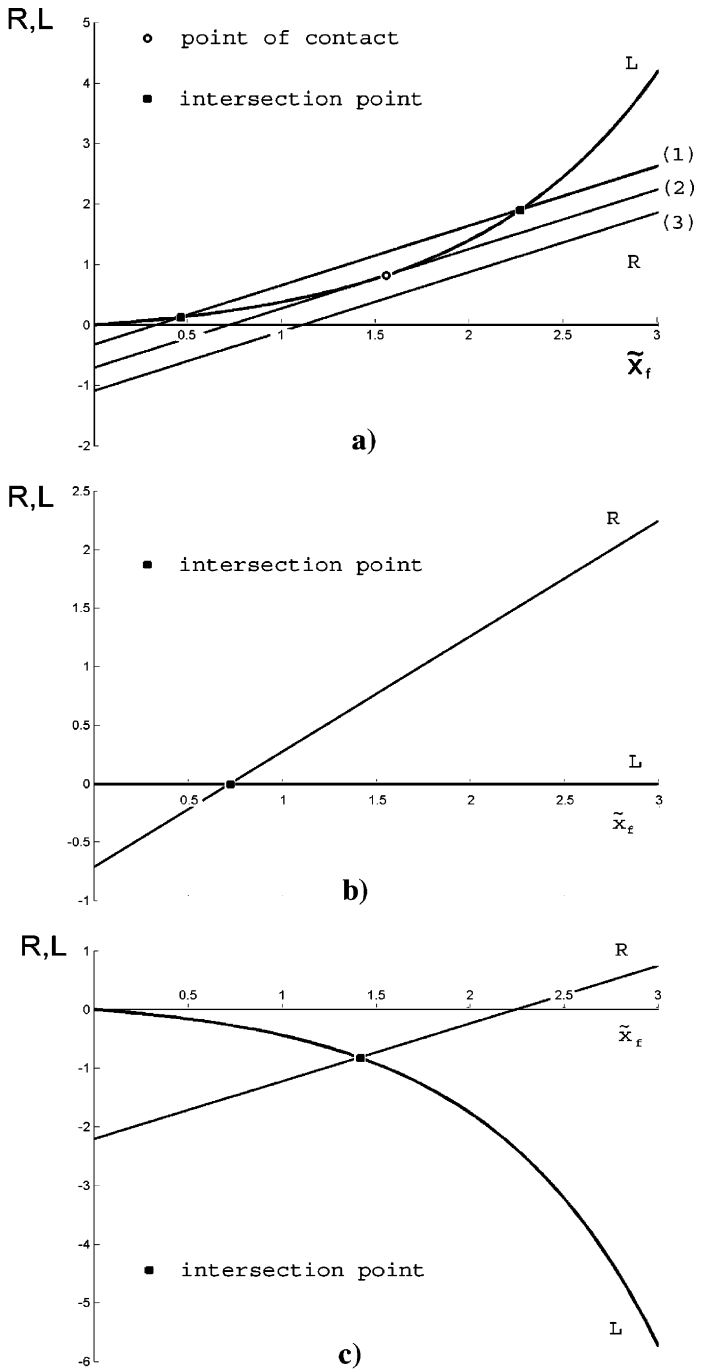

Fig. 5. Graphical analysis of Eq. (44): (a) dependence of $L(\tilde{x}_f)$—l.h.s of Eq. (44) and $R(\tilde{x}_f)$—r.h.s of Eq. (44) at $D < 0$ and any $\bar{u}_2''$ or at $D < 0$ and one of the conditions $0 < \bar{u}_2'' < \frac{1}{2} - \sqrt{D}$ or $\frac{1}{2} + \sqrt{D} < \bar{u}_2'' < 1$ (D is the discriminant of the equation $\bar{u}_2'' - 1 + (1/Pe\bar{u}_2'') = 0$); (1)–(3) correspond to various values of $\bar{u}_2'' : \bar{u}_{2(1)}'' > \bar{u}_{2(2)}'' > \bar{u}_{2(3)}''$, (b) dependence L and R upon $\tilde{x}_f$ at $D = 0$, (c) dependence L and R upon $\tilde{x}_f$ at $D < 0$ and $\frac{1}{2} - \sqrt{D} < \bar{u}_2'' < \frac{1}{2} + \sqrt{D}$.

Now the momentum and energy equations for steady flow in heated capillary are

$$\bar{u}_2' = \varphi_1(\tilde{x}_f) \tag{48}$$

$$\bar{u}_2'' = \varphi_2(\tilde{x}_f) \tag{49}$$

The stationary states correspond to parametrical equation

$$\bar{u}_2' = \bar{u}_2'', \tag{50}$$

which includes the following parameters: *Re*, *Pe*, *Fr*, v_{12}, $\overline{T}_s$, $\overline{L}$, $\tilde{l}$ and $\bar{q}_2$.

Eq. (50) postulates equality of the velocity due to liquid evaporation $\bar{u}_2''$ and the one due to the capillary and pressure forces $\bar{u}_2'$.

6. Parametrical analysis

The solution of Eq. (50) determines the steady states of the liquid velocity, as well as the position of the meniscus in a heated microchannel. Eq. (50) can have one, two or three steady solutions. This depends on the value of the parameter $\tilde{l}$ (in the generic case—parameter *B*), which takes into account the effect of the capillary forces.

Consider the possible regimes of flow corresponding to $\tilde{l} \gg 1$ and $\tilde{l} \sim 1$. We refer to the first regime as "semi-filled", whereas the second one as "filled".

The change of velocity due to liquid evaporation $\bar{u}_2''$ and influence of the capillary forces $\bar{u}_2'$ versus $\tilde{x}_f$ for $\tilde{l} \gg 1$ is illustrated in Fig. 6. In the case $\tilde{l} \gg 1$ the curves $\bar{u}_2'(\tilde{x}_f)$ and $\bar{u}_2''(\tilde{x}_f)$ have only

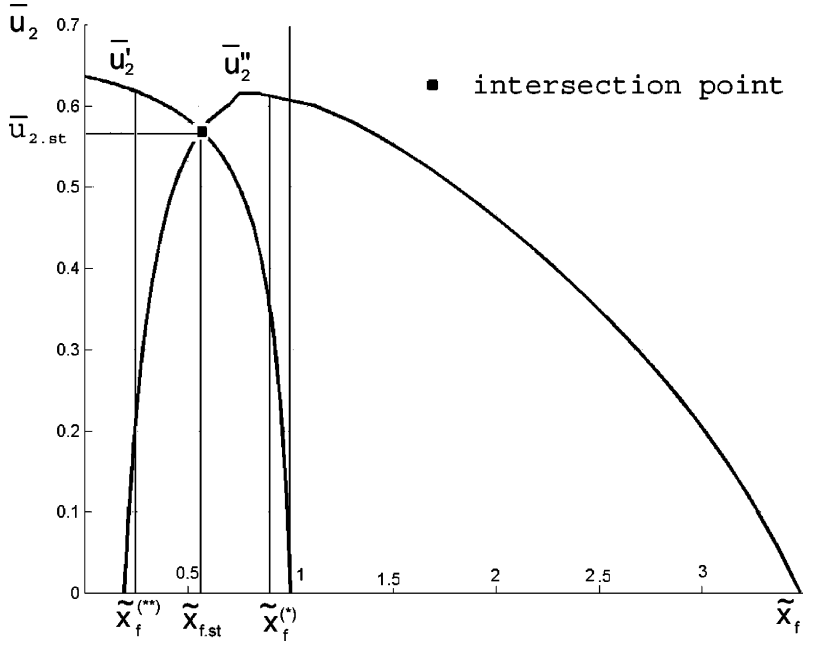

Fig. 6. Solution of Eq. (47) at $\tilde{l} \gg 1$.

one point of intersection, which determines the stationary values of $\bar{u}_2 = \bar{u}_{2.st}$ and $\tilde{x}_f = \tilde{x}_{f.st}$. It is not difficult to show that this point is stable. Indeed a displacement of the meniscus from its initial position $\tilde{x}_{f.st}$ to the position $\tilde{x}^{(*)}_{f.st}$ leads to the situation, when the velocity due to the liquid evaporation $\bar{u}''_2$ exceeds the velocity due to capillary force $\bar{u}'_2$. This leads to the return of the meniscus to its initial position. If the meniscus displaces to the left, $\bar{u}'_2 > \bar{u}''_2$, this also leads to the return of the system to its initial state.

The dependence of the stable values of the liquid velocity $\bar{u}_{2.st}$ and the meniscus location $\tilde{x}_{f.st}$ upon the Peclet number and upon the parameter A are plotted in Fig. 7. The effect of the Peclet number on $\bar{u}_{2.st}$ and $\tilde{x}_{f.st}$ is shown in Fig. 7(a). An increase in the Peclet number is accompanied by an increase in $\bar{u}_{2.st}$ and a decrease in $\tilde{x}_{f.st}$. The changing of $\bar{u}_{2.st}$ and $\tilde{x}_{f.st}$ with A is more complicated (Fig. 7(b)). An increase of A leads to a monotonous increase of $\tilde{x}_{st}$, whereas the dependence of $\bar{u}_{r.st}(A)$ has maximum at $A > A_m$, A_m corresponds to extremum of the curve $\bar{u}''_2(\tilde{x}_f)$.

Fig. 7(b) illustrates the influence of some physical parameters on the characteristics of the capillary flow. The dimensionless parameter A may be expressed as $A = (1/128)(q_e/q_w L)(\rho_* g d^3/(\nu_1 - \nu_2))$. Thus, an increase of the heat flux on the wall or the length of the capillary causes a decrease of the parameter A and is accompanied by the displacement of the meniscus near the inlet of the microchannel. When the distance $\tilde{x}_f$ between the interface and the inlet is small enough, the heat losses increase and the rate of evaporation u'_2 decreases.

The possible intersections of curves $\bar{u}'_2(\tilde{x}_f)$ and $\bar{u}''_2(\tilde{x}_f)$ at $\tilde{l} \sim 1$ are shown in Fig. 8. If the values of A are small enough ($0 < A < A_1$), there is only one intersection point P_1. It is located on the left branch of the curve $\bar{u}''_2(\tilde{x}_f)$ and corresponds to steady regime of the flow. Parameters $A = A_1$ and $A = A_3$ confine the domain within which there are three intersection points of the curves $\bar{u}'_2(\tilde{x}_f)$ and $\bar{u}''_2(\tilde{x}_f)$. One of these points (intermediate) corresponds to the unstable state. The boundary values $A = A_1$ and $A = A_3$ correspond to two intersection points, one of which is the point of touch. If $A > A_3$ there is only one intersection point (stable). The domains of existence of one, two or three solutions of Eq. (50) are shown in Figs. 9 and 10 in the plane of the parameters $A - Pe$ and the space $A - Pe - \bar{x}_{f.cap}$. The existence of two stable regimes of flow (with fixed values of the parameters and various meniscus positions) may be explained as follows: when the meniscus is located near the outlet, the volume of the capillary is filled by liquid. Since the length of the vapor region is very small, the friction force due to vapor is negligible. The friction force due to liquid is smaller than the gravity force. Thus, the capillary force is balanced mainly by the gravity force. At the same time, dynamic equilibrium is possible, when friction forces due to vapor is dominant. This situation appears, when the meniscus approaches the inlet of the microchannel and the gravity force together with the friction force due to the liquid are negligible.

Thus, depending upon the values of the parameter $\tilde{l}$ we can classify the equilibrium states, using parameter A (Table 1). When $A = A_1$ or $A = A_3$ the curves $\bar{u}'_2$ and $\bar{u}''_2$ are tangent.

The stable stationary states that correspond to two lower rows in Table 1 may be subdivided in two groups: gravity and friction; it depends on the dominant factor. The first of them corresponds to the conditions when the capillary force due to surface tension is compensated mainly by the weight of liquid column, whereas the second one corresponds to the dominant role of the friction force due to the vapor flow.

Table 1 shows that only one stationary state is possible, when the meniscus is far enough from the outlet of the capillary. Contrary to this, when the capillary is 'filled', namely, the interface surface is near the outlet, two and three stationary states are possible. From the physical point of

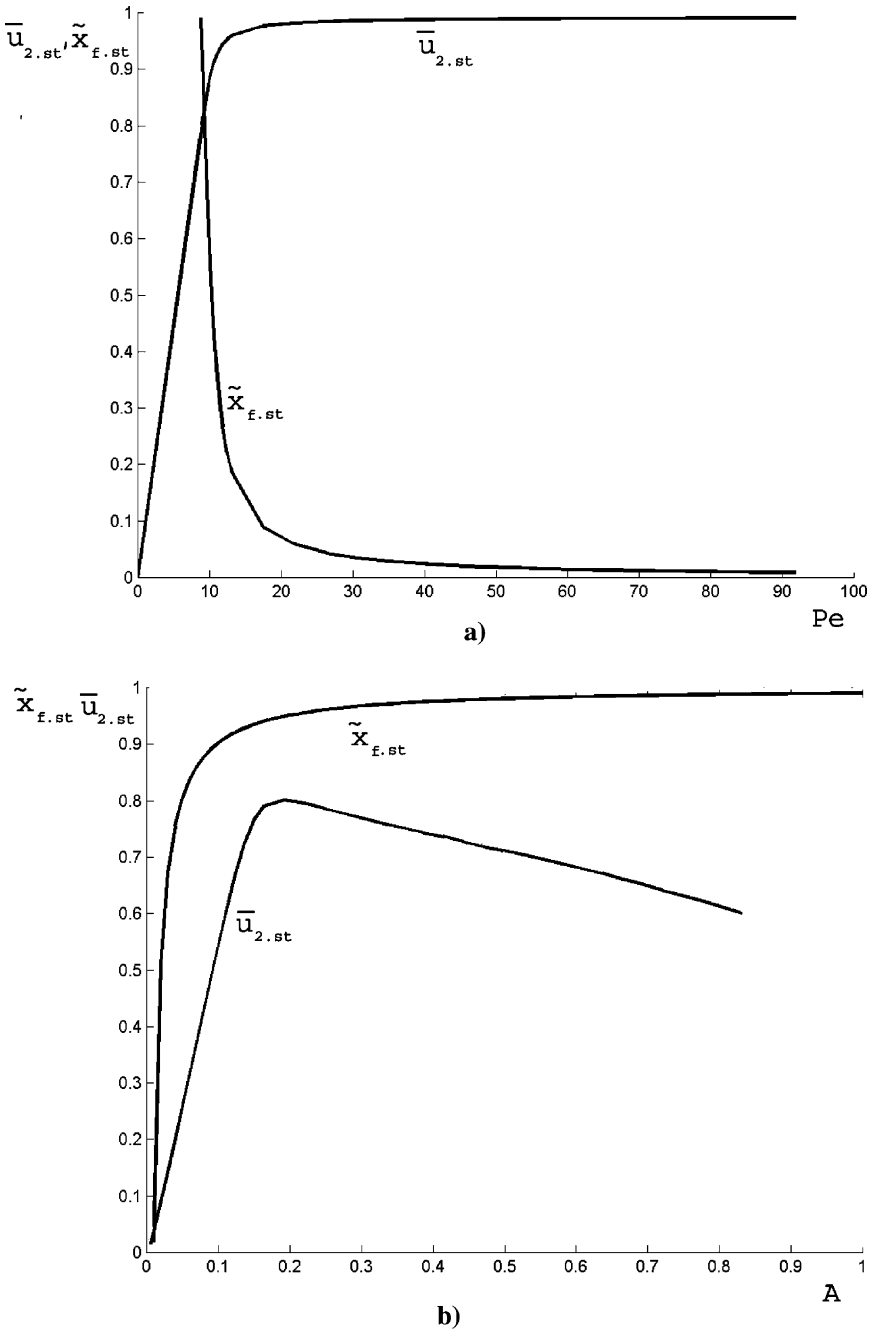

Fig. 7. Dependence of liquid velocity $\bar{u}_{2.st}$ and meniscus location $\tilde{x}_{f.st}$ versus Peclet number and parameter A (semi-filled regime): (a) $u''_{2.st}(Pe); \tilde{x}_{f.st}(Pe)$, (b) $u''_{2.st}(A); \tilde{x}_{f.st}(A)$.

view, these phenomena may be explained by the different contribution of the friction force due to the vapor. In the first case this force is dominant, whereas in the second one its effect is negligible.

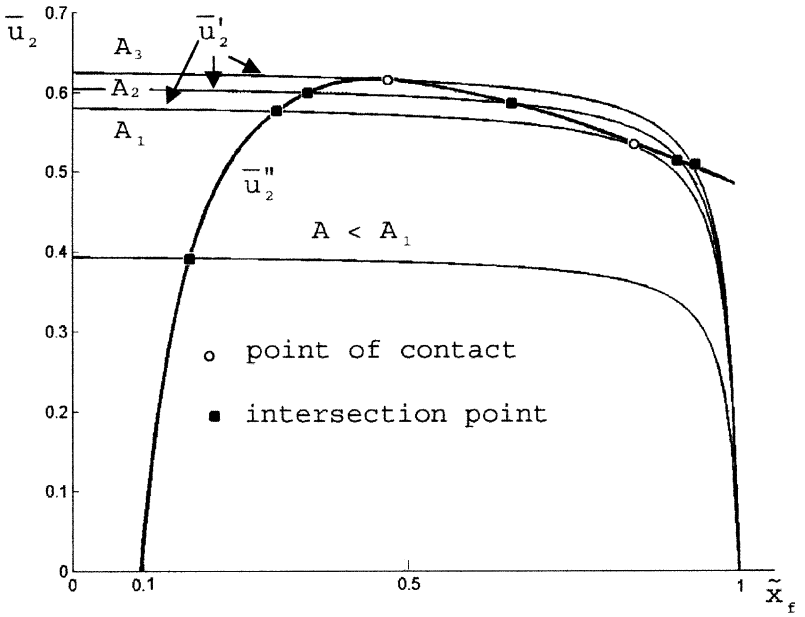

Fig. 8. Solution of Eq. (47) at $\tilde{l} \sim 1$.

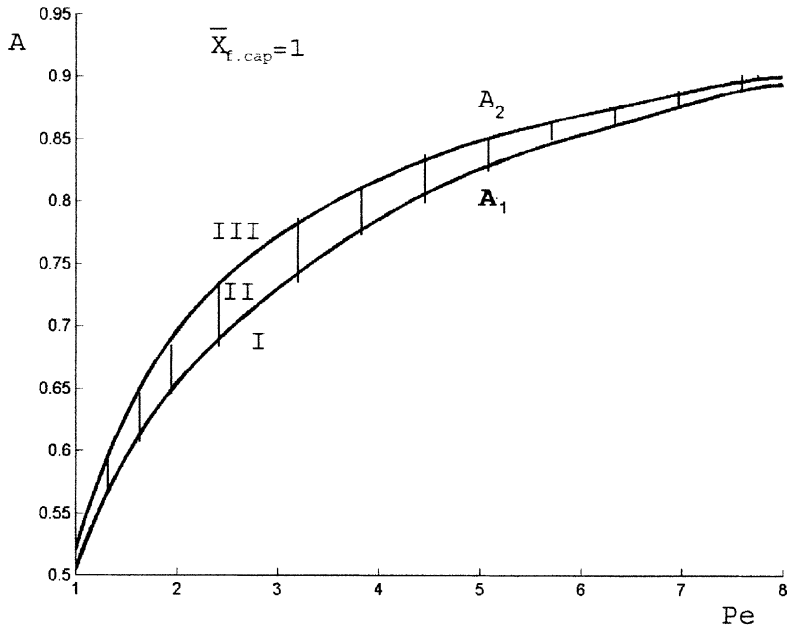

Fig. 9. Diagram of steady states: I and III—domains of existence of single solution, II—domain of existence of three solutions (two stable and one unstable), Lines A_1 and A_2 correspond to two stable solutions.

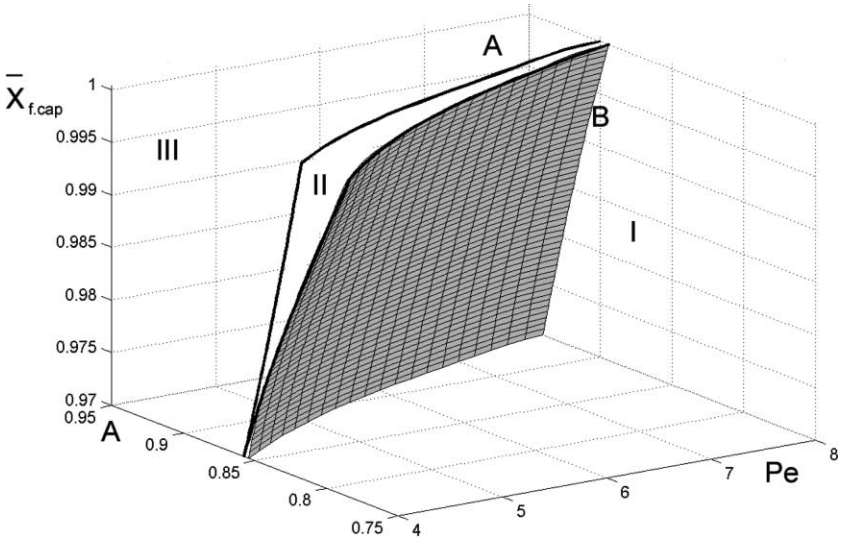

Fig. 10. Three-dimensional diagram of steady states: I and III—domains of existence of single solution, II—domain of existence of three solutions (two stable and one unstable), Boundary surfaces correspond to two stable solutions.

Table 1

Regime	Parameter		Number of stationary states	Stability
	$\tilde{l}$	A		
Semi-filled	$\tilde{l} \gg 1$	$0 < A < \infty$	One	Stable
Filled	$\tilde{l} \sim 1$	$0 < A < A_1$	One	Stable
		$A_1 < A < A_3$	Three	Two stable, one unstable
		$A = A_1$	Two	Stable
		$A = A_3$		

7. Results and discussion

The numerical calculations of the liquid velocity and the meniscus position were carried out for the various wall heat flux q_w, the acceleration due to gravity g, as well as the length and the diameter of the microchannel in the ranges $(200 < q_w < 2000)$ W/m^2, $(5 < g < 45)$ m/s^2, $(0.015 < L < 0.05)$ m, $(0.1 < d < 2)$ 10^{-4} m. The change of the flow velocity and meniscus position versus heat flux is illustrated by Fig. 11. An increase in q_w is accompanied by a decrease in the $x_{f.st}$ and growing of the outlet $u_{2.st}$. The sharp change of $x_{f.st}$ and $u_{2.st}$ is observed at relatively small heat fluxes when the meniscus is located at a away from the inlet and heat losses are negligible. In this case all the energy which is supplied to the liquid is used for its evaporation so that its velocity is directly proportional to q_w. The character of the process changes qualitatively when

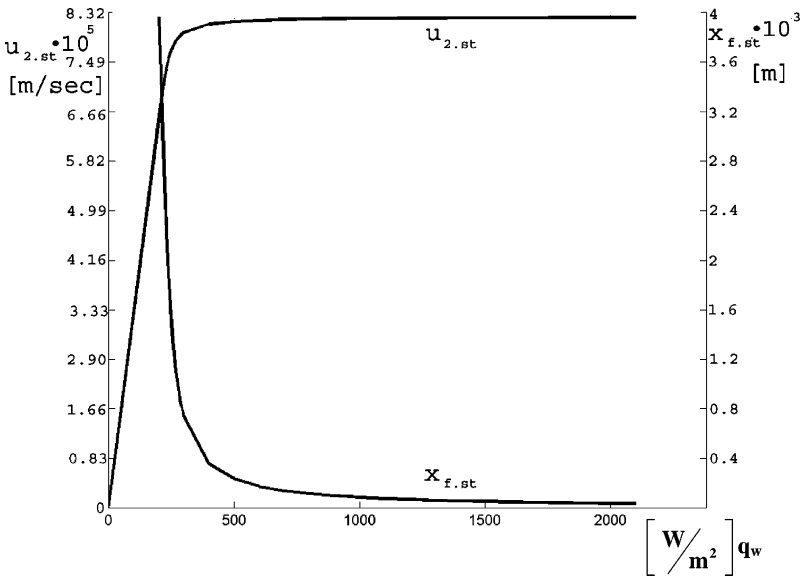

Fig. 11. Stable liquid velocity and meniscus location versus heat flux on the microchannel wall ($L = 2 \times 10^{-2}$ m, $d = 10^{-4}$ m, $g = 9.8$ m/s^2).

q_w is much greater. When the meniscus approaches the inlet cross-section, the heat losses became significant, because they are proportional to $(\overline{T}_s - 1)/\tilde{x}_f$. In this case an increase in q_w is accompanied by an increase in the heat losses to the inlet and practically has no effect on the liquid velocity.

The effect of the acceleration due to gravity on the steady state liquid velocity and the meniscus position is shown in Fig. 12. An increase in g is accompanied by the displacement of the meniscus toward the inlet and a decrease in the liquid velocity.

Fig. 13 illustrates the effect of the microchannel length on $u_{2.st}$ and $x_{f.st}$. It may be seen, that an increase in the microchannel length is accompanied by a monotonous decrease in $x_{f.st}$, whereas the function $u_{2.st}(L)$ has a maximum. Such a type of dependence of $u_{2.st}(L)$ is due to opposite features: (a) the growth of the friction forces with L; (b) the growth of the total heat flux to the liquid. When L is relatively small the increase in the total heat flux plays the dominant role, which leads to an increase in the liquid velocity. When L is large enough, the hydraulic resistance of the vapor region is dominant. Its growth leads to the displacement of the meniscus towards the inlet, the increase in the heat losses and the decrease in the liquid velocity.

The graphs of the functions $u_{2.st}(d)$ and $x_{f.st}(d)$ are plotted in Fig. 14. Both curves have rising and falling branches and accordingly characteristic maximum at certain (depending on the curve) value of the microchannel diameter. When $d > 1 \times 10^{-4}$ m the liquid velocity is inversely proportional to d. Within this regime an increase in the microchannel diameter leads to a significant decrease in the friction force, as well as the forces due to the surface tension. Under these conditions the length of the liquid region is shortened. The situation changes qualitatively when $x_{f.st}$ is small enough and heat losses play significant role. In this case the growth of $u_{2.st}$ with d takes place.

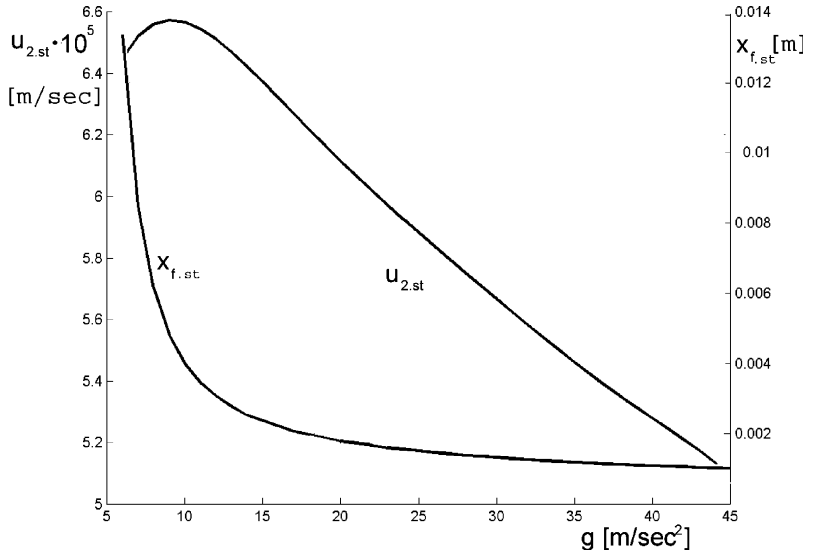

Fig. 12. Stable liquid velocity and meniscus location versus gravity acceleration ($L = 2 \times 10^{-2}$ m, $d = 10^{-4}$ m, $q_w = 200\ \frac{W}{m^2}$).

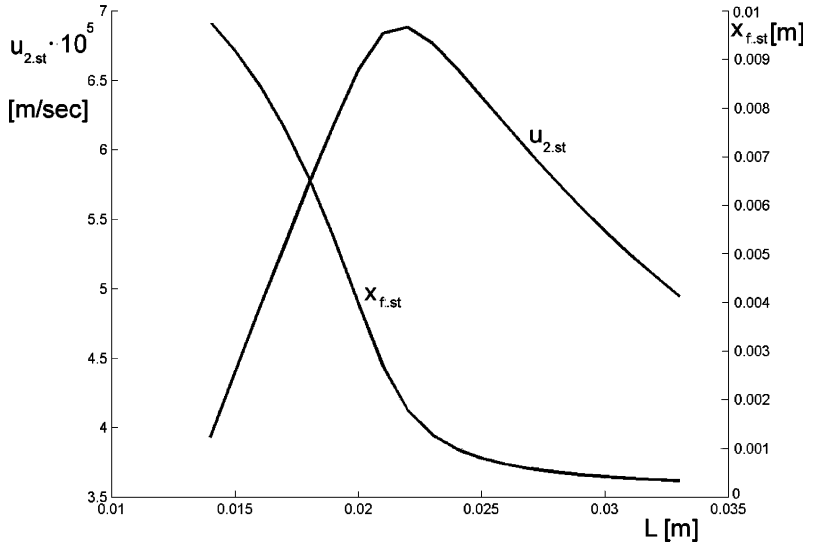

Fig. 13. Liquid velocity and the location of the meniscus versus capillary length ($d = 10^{-4}$ m, $g = 9.8$ m/s^2, $q_w = 200\ \frac{W}{m^2}$).

8. The efficiency of the cooling system

The total energy, which is supplied to the liquid from the wall, is equal to the heat flux q_w, multiplied by the lateral area of the microchannel: $\pi d L q_w$. The energy, which is expended to the liquid vaporization, is equal to the latent heat of evaporation q_e, multiplied by the mass liquid flow-rate through a cross-section of the microchannel, and is equal $\rho_2 u_2 (\pi d^2/4) q_e$.

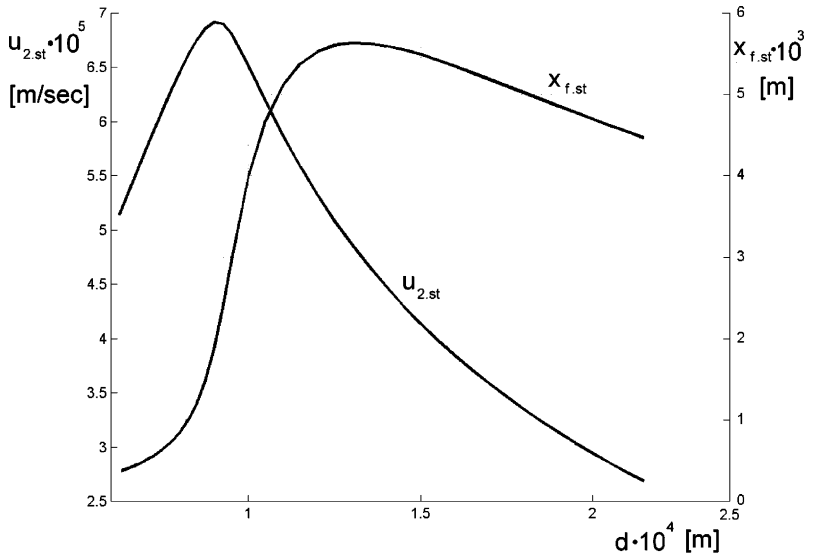

Fig. 14. Liquid velocity and meniscus location versus capillary diameter ($= 2 \times 10^{-2}$ m, $g = 9.8$ m/s^2, $q_w = 200$ $\frac{W}{m^2}$).

The effect of the heat losses to the inlet, on the thermal states of the microchannel, depends mainly on the meniscus position which is determined by the flow parameters. To characterize this effect, the coefficient of efficiency is introduced; it may be defined as the ratio of the energy expending to the liquid vaporization and the total energy supplied to the microchannel.

$$\eta = \frac{\rho_2 u_2 d q_e}{4 q_w L} \tag{51}$$

Since the coefficient of efficiency depends on the location of the meniscus, it is different for semi-filled and filled regimes.

In a steady state, two-phase flow in a heated capillary, there is the balance of forces, which act on the liquid and its vapor. The analysis of this balance shows, that there are two stable states of the flow. They correspond to the different locations of the meniscus, which separates the liquid and the vapor. The existence of such states may be explained by the changes in the values of the different components in the balance equation. When the meniscus is near the outlet, the gravity and the surface tension play the main role, whereas the friction forces of the liquid and the vapor are negligible. In contrast, when the meniscus is near the inlet, the friction and surface tension forces are the main ones.

The position of the meniscus within the microchannel defines the type of the temperature distribution. In the first case, when the meniscus is near the outlet, the temperature gradient of the vapor region is small. The rate of evaporation is determined mainly by the heat flux in the liquid region. Therefore, the necessary condition of the evaporation consists of the existence of the region (near the meniscus), where the water is overheated (its temperature is higher then the temperature of boiling). The heat losses to the inlet tank cause the existence of the temperature maximum.

When the meniscus is near the inlet of the microchannel, the heat losses increase, because the gradient of the temperature is greater.

Thus, there are two meniscus positions near the edges of the microchannel, where the heat losses are significant. Between them there is some position, in which these losses are minimal and

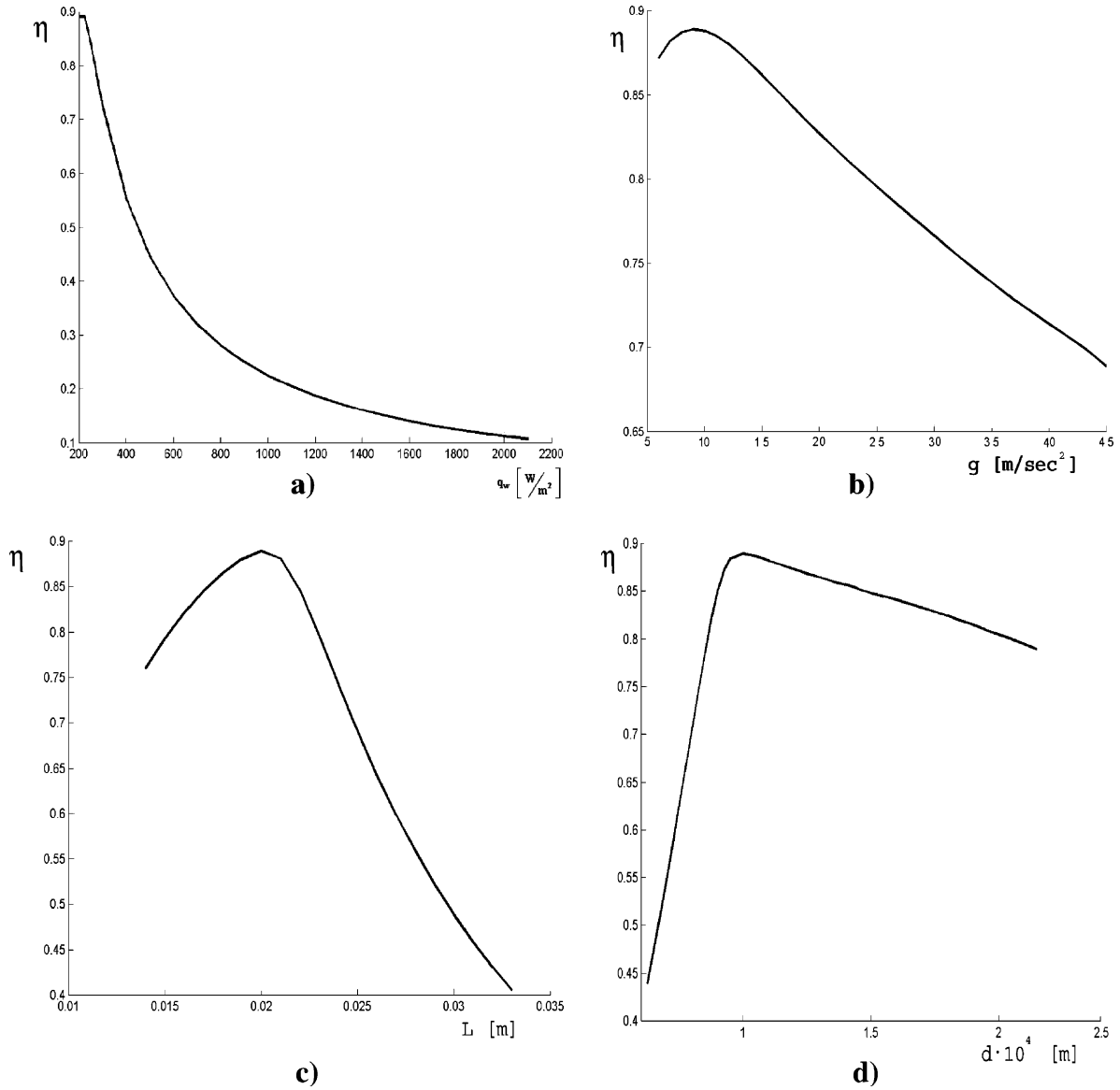

Fig. 15. Efficiency of cooling system (friction regime): (a) coefficient of efficiency versus heat flux, (b) coefficient of efficiency versus gravity, (c) coefficient of efficiency versus capillary length, (d) coefficient of efficiency versus capillary diameter.

the evaporation is the most intensive. This corresponds to the optimal efficiency of the cooling system.

The effect of various parameters on the efficiency coefficient is illustrated in Fig. 15(a)–(d). It may be seen, that an increasing of heat flux on the wall leads to a significant decrease in η. It is due to the meniscus displacement towards the inlet and growth of heat losses into the cooling liquid. The calculations show (Fig. 15(a), (c)) that for given values of parameters there is some "optimal" values of microchannel's diameter and length, at which the coefficient of efficiency reaches maximum.

9. Conclusions

A theory of two-phase laminar flow with a distinct interface has been developed. Although this theory is based on a one-dimensional approximation, it takes into account the major features of the process: the inertia, gravity, surface tension and friction forces. Thus this study may be expected to give the physically realistic pattern of a laminar flow in a heated microchannel. This allows one to use the present theory to study the regimes of flow, as well as optimizing a cooling system of electronic devices with high power densities.

Partial results are as follows:

1. The problem of a flow in a heated microchannel with distinct interphase is formulated.
   To calculate the flow parameters under the conditions when the meniscus position and the liquid velocity at the inlet are unknown 'a priori'. The mass, momentum and energy equations are used for both phases, as well as the balance conditions at the interphase. The integral condition which connects flow parameters at the inlet and the outlet cross-sections is derived.
2. The analytical solution of the problem is obtained.
   It is shown that the rate of vaporization (the liquid's velocity), the liquid and vapor temperatures, the position of the meniscus in the microchannel, its hydraulic resistance and the thermal losses are determined by eight non-dimensional groups, accounting for the effects of heat transfer, phase change, as well as inertia, friction, surface tension and gravity forces. The number of such non-dimensional groups may be reduced to 4 by introducing a general parameter: the capillary height, which depends on the Weber, Froude and Euler numbers.
3. The parametrical analysis of the problem was done. The classification of possible regimes of flow are proposed. It is based on non-dimensional parameter accounting for the ratio of the microchannel length to the capillary height. It is shown that in the generic case the governing system of equations that describes capillary flow has three stationary solutions: two stable and one (intermediate)—unstable.
4. It is shown, that an increase in the heat flux is accompanied by an increase in the liquid and vapor velocities, the meniscus displacement towards the outlet cross-section, as well as growth of vapor to liquid forces ratio and heat losses. When q_w is large enough, the difference between the intensity of heat transfer and heat losses are limited by some final value which determines the maximum rate of vaporization. Accordingly, when q_w is large all characteristic parameters are practically invariable.

5. It is shown that the existence of two stable states (at given values of the operating parameters) is due to the dominant role of the gravity or friction forces at the various meniscus positions. A decrease in the gravity leads to the displacement of the meniscus toward the outlet and to a decrease in the heat losses and an increase in the liquid and vapor velocities. A decrease in the microchannel diameter leads to a monotonous increase in the liquid and vapor velocities, whereas the dependence of the meniscus position versus d has an extremum.
6. At given values of the parameters, there are optimal values of the microchannel diameter and length, which correspond to a maximum efficiency coefficient.

Acknowledgements

L.A. Ekelchik was supported by a grant from The Center for Absorption in Science of the Ministry of Immigrants Absorption State of Israel.

L.P. Yarin is supported by The Israel Council for Higher Education.

Appendix A. The dependence between the saturation pressure and temperature

The dependence of the saturation pressure $P_{1.s}$ and temperature T_s the for several liquids is determined by Antoine equation (Reid et al., 1987). We use the following expression for water and its vapor under atmospheric pressure (Seaver et al., 1989):

$$P_s = a_0 + t_s[a_1 + t_s(a_2 + t_s\{a_3 + t_s[a_4 + t_s(a_5 + a_6 t_s)]\})], \tag{A.1}$$

where

$$a_0 = 6.107799961 \times 10^{-2}, \quad a_1 = 4.436518521 \times 10^{-3}, \quad a_2 = 1.428945805 \times 10^{-4},$$
$$a_3 = 2.650648731 \times 10^{-6}, \quad a_4 = 3.031240396 \times 10^{-8}, \quad a_5 = 2.034080948 \times 10^{-10},$$
$$a_6 = 6.136820929 \times 10^{-13},$$

t is measured in Celsius.

From Eq. (A.1) it follows that

$$\frac{dT_s}{dP_s} = \frac{1}{a_1 + t_s(2a_2 + t_s\{3a_3 + t_s[4a_4 + t_s(5a_5 + 6a_6 t_s)]\})}$$

For $t_s = 100$ °C

$$\frac{dT_s}{dP_s} = 2.6859 \times 10^{-4}$$

for $t_s = 200$ °C

$$\frac{dT_s}{dP_s} = 2.4066 \times 10^{-5}$$

This shows that T_s changes weakly with the pressure. This allows us to neglect the dependence of the hydraulic resistance of the vapor on the saturation temperature T_s and assume that it is determined by the external pressure $P_{1.00}$.

Appendix B. Integral relations

(A) Integrating Eq. (2) from 0 to $x_{f(-)}$ we obtain

$$\int_0^{x_f}\left(\frac{\partial\rho_2}{\partial t}+\frac{\partial\rho_2 u_2}{\partial x}\right)dx=\frac{\partial}{\partial t}\int_0^{x_f}\rho_2\,dx-\rho_{2.f}\frac{dx_f}{dt}+\{(\rho_2u_2)_f-(\rho_2u_2)_0\}=0 \tag{B.1}$$

Integrating Eq. (2) from $x_{f(+)}$ to L yields

$$\int_{x_f}^{L}\left(\frac{\partial\rho_1}{\partial t}+\frac{\partial\rho_1 u_1}{\partial x}\right)dx=\frac{\partial}{\partial t}\int_{x_f}^{L}\rho_1\,dx+\rho_{1.f}\frac{dx_f}{dt}+\{(\rho_1u_1)_{00}-(\rho_1u_1)_f\}=0 \tag{B.2}$$

Summing Eqs. (B.1) and (B.2) we get

$$\frac{\partial}{\partial t}\left(\int_0^{x_f}\rho_2\,dx+\int_{x_f}^{L}\rho_1\,dx\right)+(\rho_1-\rho_2)_f\frac{dx_f}{dt}+\{[(\rho_2u_2)_f-(\rho_2u_2)_0]+[(\rho_1u_1)_{00}-(\rho_1u_1)_f]\}=0 \tag{B.3}$$

From Eq. (11) it follows that

$$(\rho_1u_1-\rho_2u_2)_f=(\rho_1-\rho_2)_fV_f=(\rho_1-\rho_2)_f\frac{dx_f}{dt} \tag{B.4}$$

Then Eq. (B.3) takes the following form

$$\frac{\partial}{\partial t}\left(\int_0^{x_f}\rho_2\,dx+\int_{x_f}^{L}\rho_1\,dx\right)+(\rho_{1.00}u_{1.00}-\rho_{2.0}u_{2.0})=0 \tag{B.5}$$

(B) Multiplying Eq. (2) by u_i and summing that equation with Eq. (3) we obtain the equation

$$\frac{\partial\rho_iu_i}{\partial t}+\frac{\partial\rho_iu_i^2}{\partial x}=-\frac{\partial P_i}{\partial x}-\rho_ig-\frac{\partial F_i}{\partial x} \tag{B.6}$$

Integrating Eq. (B.6) from 0 to x_f and from x_f to L yields

$$\frac{\partial}{\partial t}\int_0^{x_f}\rho_2u_2\,dx-(\rho_2u_2)_f\frac{dx_f}{dt}+\{(\rho_2u_2^2)_f-(\rho_2u_2^2)_0\}=(P_{2.0}-P_{2.f})-g\int_0^{x_f}\rho_2\,dx-F_{2.f} \tag{B.7}$$

$$\frac{\partial}{\partial t}\int_{x_f}^{L}\rho_1u_1\,dx+(\rho_1u_1)_f\frac{dx_f}{dt}+\left\{(\rho_1u_1^2)_{00}-(\rho_1u_1^2)_f\right\}=(P_{1.f}-P_{1.00})-g\int_{x_f}^{L}\rho_1\,dx-F_{1.00} \tag{B.8}$$

Note that we account for that $F_{2.0}\equiv 0$, $F_{1.f}\equiv 0$ in Eqs. (B.7) and (B.8). Summing Eqs. (B.7) and (B.8), we obtain

$$\begin{aligned}&\frac{\partial}{\partial t}\left(\int_0^{x_f}\rho_2u_2\,dx+\int_{x_f}^{L}\rho_1u_1\,dx\right)+(\rho_1u_1-\rho_2u_2)\frac{dx_f}{dt}+\left\{(\rho_2u_2^2)_f-(\rho_2u_2^2)_0+(\rho_1u_1^2)_{00}-(\rho_1u_1^2)_f\right\}\\&\quad=(P_{2.0}-P_{2.f}+P_{1.f}-P_{1.00})-g\left(\int_0^{x_f}\rho_2\,dx+\int_{x_f}^{L}\rho_1\,dx\right)-(F_{2.f}+F_{1.00})\end{aligned} \tag{B.9}$$

Using the conditions (12) and (13), we transform Eq. (B.9). Taking into account Eq. (B.4), we rewrite (13) as follows

$$(\rho_1 u_1^2 - \rho_2 u_2^2)_{\mathrm{f}} = f_{\mathrm{L}} - (P_1 - P_2)_{\mathrm{f}} + (\rho_1 - \rho_2)_{\mathrm{f}} \left(\frac{\mathrm{d}x_{\mathrm{f}}}{\mathrm{d}t} \right)^2 \tag{B.10}$$

Then Eq. (B.9) takes form

$$\frac{\partial}{\partial t} \left(\int_0^{x_{\mathrm{f}}} \rho_2 u_2 \, \mathrm{d}x + \int_{x_{\mathrm{f}}}^{L} \rho_1 u_1 \, \mathrm{d}x \right) = f_{\mathrm{L}} - [(\rho_1 u_1^2)_{00} - (\rho_2 u_2^2)_0] + (P_{2.0} - P_{1.00}) - g \left(\int_0^{x_{\mathrm{f}}} \rho_2 \, \mathrm{d}x + \int_{x_{\mathrm{f}}}^{L} \rho_1 \, \mathrm{d}x \right) - (F_{2.\mathrm{f}} + F_{1.00}) \tag{B.11}$$

(C) Rewrite Eq. (4) in the following form and integrate this equation from 0 to x_{f} and from x_{f} to L:

$$\frac{\partial}{\partial t} \int_0^{x_{\mathrm{f}}} \rho_2 h_2 \, \mathrm{d}x - (\rho_2 h_2)_{\mathrm{f}} \frac{\mathrm{d}x_{\mathrm{f}}}{\mathrm{d}t} + \{(\rho_2 h_2 u_2)_{\mathrm{f}} - (\rho_2 h_2 u_2)_0\} = \lambda_2 \left(\frac{\partial T_2}{\partial x} \right)_{\mathrm{f}} - \lambda_2 \left(\frac{\partial T_2}{\partial x} \right)_0 + q x_{\mathrm{f}} \tag{B.12}$$

$$\frac{\partial}{\partial t} \int_{x_{\mathrm{f}}}^{L} \rho_1 h_1 \, \mathrm{d}x + (\rho_1 h_1)_{\mathrm{f}} \frac{\mathrm{d}x_{\mathrm{f}}}{\mathrm{d}t} + \{(\rho_1 h_1 u_1)_{00} - (\rho_1 h_1 u_1)_{\mathrm{f}}\} = \lambda_1 \left(\frac{\partial T_1}{\partial x} \right)_{00} - \lambda_1 \left(\frac{\partial T_1}{\partial x} \right)_{\mathrm{f}} + q(L - x_{\mathrm{f}}) \tag{B.13}$$

Summing Eqs. (B.12) and (B.13) we find

$$\frac{\partial}{\partial t} \left(\int_0^{x_{\mathrm{f}}} \rho_2 h_2 \, \mathrm{d}x + \int_{x_{\mathrm{f}}}^{L} \rho_1 h_1 \, \mathrm{d}x \right) + (\rho_1 h_1 - \rho_2 h_2)_{\mathrm{f}} \frac{\mathrm{d}x_{\mathrm{f}}}{\mathrm{d}t} + \{(\rho_2 h_2 u_2)_{\mathrm{f}} - (\rho_2 h_2 u_2)_0 + (\rho_1 h_1 u_1)_{00} - (\rho_1 h_1 u_1)_{\mathrm{f}}\} = \lambda_2 \left(\frac{\partial T_2}{\partial x} \right)_{\mathrm{f}} - \lambda_2 \left(\frac{\partial T_2}{\partial x} \right)_0 + \lambda_1 \left(\frac{\partial T_1}{\partial x} \right)_{00} - \lambda_1 \left(\frac{\partial T_1}{\partial x} \right)_{\mathrm{f}} + qL \tag{B.14}$$

Using Eq. (14) we obtain

$$\frac{\partial}{\partial t} \left(\int_0^{x_{\mathrm{f}}} \rho_2 h_2 \, \mathrm{d}x + \int_{x_{\mathrm{f}}}^{L} \rho_1 h_1 \, \mathrm{d}x \right) + \{(\rho_1 h_1 u_1)_{00} - (\rho_2 h_2 u_2)_0\} = -\lambda_2 \left(\frac{\partial T_2}{\partial x} \right)_0 + \lambda_1 \left(\frac{\partial T_1}{\partial x} \right)_{00} + qL \tag{B.15}$$

Appendix C. Analysis of the equations

(1) Let us transform the momentum Eq. (43) to the form:

$$\bar{u}_2' = A \frac{1 - \tilde{x}_{\mathrm{f}}}{B - \tilde{x}_{\mathrm{f}}} \tag{C.1}$$

where

$$A = \frac{Re}{32Fr\overline{L}(v_{12}-1)}, \quad B = \widetilde{L}\frac{v_{12}}{v_{12}-1}, \quad \tilde{x}_f = \bar{x}_f/\overline{X}_{fcap}, \quad \tilde{l} = \overline{L}/\overline{X}_{fcap}.$$

If the pressure is moderate ($P < 10^6$ Pa), the ratio of the kinetic viscosities of the vapor and the liquid v_{12} has the order of 70 (Johnson, 1998). The curve $\bar{u}_2'(\tilde{x}_f)$ is a hyperbola with the horizontal asymptote $\bar{u}_2' = A$ and the vertical one $\tilde{x}_f = B$ (Fig. 4(a)). The physical meaning has only the sector of lower branches of the hyperbola, which is between the lines $\tilde{x}_f = 0$ and $\tilde{x}_f = 1$. It corresponds to the position of the meniscus inside the microchannel.

(2) Now let us consider the energy Eq. (44). To reveal the shape of the curve $\bar{u}_2''(\tilde{x}_f)$ we consider its intersection with the lines $\bar{u}_2'' = \text{const}$. Write down Eq. (44) as follows:

$$\left(\bar{u}_2'' - 1 + \frac{1}{Pe\,\bar{u}_2''}\right)\left[\exp\left(Pe\overline{X}_{fcap}\tilde{x}_f\bar{u}_2''\right) - 1\right] = \overline{X}_{fcap}\tilde{x}_f - \bar{q}_2\bar{u}_2''(\overline{T}_s - 1) \tag{C.2}$$

The r.h.s. of Eq. (C.2): R is the linear function of $\bar{x}_f$. An increasing of $\bar{u}_2''$ leads to the displacement of these lines downwards. The l.h.s. of Eq. (C.2): L is non-linear function of $\tilde{x}_f$. Its sign depends on sign of the multiplier $(\bar{u}_2'' - 1 + (1/Pe\,\bar{u}_2''))$ i.e. on the determinant $D = (1/4) - (1/Pe)$. There are three cases: $D < 0$, $D = 0$, $D > 0$.

(a) $D < 0$ ($Pe < 4$). In this case $\bar{u}_2'' - 1 + (1/Pe\,\bar{u}_2'') > 0$. Since the expression in square brackets is positive, the l.h.s. of Eq. (C.2) is also positive (Fig. 5(a)). The derivatives of functions in l.h.s. and r.h.s. of Eq. (C.2) at the point $\tilde{x}_f = 0$ equal respectively

$$L' = \overline{X}_{fcap} + Pe\overline{X}_{fcap}(\bar{u}_2'' - 1)\bar{u}_2'' \tag{C.3}$$

$$R' = \overline{X}_{fcap} \tag{C.4}$$

Since $\bar{u}_2'' < 1$ then $R' > L'$. That means, that depending on value of $\bar{u}_2''$ there are one or two intersection points of the curves $L(\tilde{x}_f)$ and $R(\tilde{x}_f)$. Under certain conditions the intersection points are absent. Thus, the curve $\bar{u}_2''(\tilde{x}_f)$ has the shape as shown in Fig. 5(a).

(b) $D = 0$ ($Pe = 4$, $\bar{u}_2'' = \frac{1}{2}$). In this case there is a single intersection point of the curve $\bar{u}_2''$ with the axis of abscissa $\tilde{x}_f = (\bar{q}_2(\overline{T}_s - 1))/2\overline{X}_{fcap}$ (Fig. 5(b)).

(c) $D > 0$ ($Pe > 4$). When $\bar{u}_2''$ change within the range $\frac{1}{2} - \sqrt{D} \leqslant \bar{u}_2'' \leqslant \frac{1}{2} + \sqrt{D}$, $L(\tilde{x}_f)$ decreases with the increasing of $\tilde{x}_f$. In this case there is one intersection point (Fig. 5(c)). When $0 < \bar{u}_2'' < \frac{1}{2} - \sqrt{D}$ or $\frac{1}{2} + \sqrt{D} < \bar{u}_2'' < 1$ i.e. $\bar{u}_2'' - 1 + (1/Pe\,\bar{u}_2'') > 0$ and there are two intersection points as it is shown in Fig. 5(a).

Now we find intersection points of the curve $\bar{u}_2''(\tilde{x}_f)$ with the abscissa axis. Assuming in Eq. (B.2) $\bar{u}_2'' \to 0$ (at finite $\bar{x}_f$), we obtain

$$(\tilde{x}_f)_{1,2} = \frac{1}{\overline{X}_{fcap}} \pm \frac{1}{\overline{X}_{fcap}}\sqrt{1 - 2\frac{\bar{q}_2(\overline{T}_s - 1)}{Pe}} \tag{C.5}$$

The dependances $\bar{u}_2''(\tilde{x}_f)$ for various Pe are plotted in Fig. 4(b). The shape of these curves significantly depends on the value of the Peclet number. When $Pe < 4$ the raising and the falling branches of $\bar{u}_2''(\tilde{x}_f)$ contain points $(\tilde{x}_f)_1$ and $(\tilde{x}_f)_2$ on the abscissa axis and form canopy-shape

curves with characteristic maximum depending on Pe. Contrary to that if $Pe \geqslant 4$, the curves $\bar{u}_2''(\tilde{x}_f)$ are not continuous. When $\tilde{x}_f$ is large, the upper and lower branches have one ($Pe = 4$) or two ($Pe > 4$) asymptotes.

References

Bowers, X.B., Mudawar, I., 1994. High flux boiling in low flow rate, low pressure drop minichannel and microchannel heat sink. Int. J. Heat Mass Transf. 37, 321–333.

Ghiaasiaan, S.M., Abdel-Khalik, S.I., 2001. Two-phase flow in microchannels. Adv. Heat Transf. 34, 145–253.

Grigoriev, V.A., Zorin, V.M. (Eds.), 1982. Heat and Mass Transfer. Thermal Experiment Reference Book. Energoizdat, Moscow (in Russian).

Ha, J.M., Peterson, G.P., 1998. Capillary performance of evaporating flow in microgrooves. An approximate analytical approach for very small tilt angles. Trans. ASME, J. Heat Transf. 120, 452–457.

Incropera, F.P., 1999. Liquid cooling of electronic devices by single-phase convection. John Wiley and Sons. 1. NC, New York.

Johnson, R.W. (Ed.), 1998. The Handbook of Fluid Dynamics, Appendix C. Properties of Gases and Vapors. CRC Press, Boston.

Khrustalev, D., Faghri, A., 1995. During evaporation on capillary-grooved structures of heat pipes. Trans. ASME, J. Heat Transf. 117, 740–746.

Landau, L.D., Lifshiz, E.M., 1959. Fluid Mechanics, second ed. Pergamon, London.

Landerman, C.S., 1994. Microchannel flow boiling mechanisms leading to burnout. J. Heat Transfer Electron Syst. ASME-HTD 292, 124–136.

Levich, V.G., 1962. Physicochemical Hydrodynamics. Prentice Hall, London.

Morijama, K., Inoue, A., 1992. The thermohydraulic characteristics of two-phase flow in extremely narrow channels (the frictional pressure drop and heat transfer of boiling two-phase flow, analytical model). Heat Transfer Jpn. Res. 21, 838–856.

Peles, Y.P., Yarin, L.P., Hetsroni, G., 1998. Heat transfer of two-phase flow in a heated capillary. Heat Transfer 1998, Proceeding of the 11th International Heat Transfer Conference, 2, Kuongju, Korea, pp. 193–198.

Peles, Y.P., Yarin, L.P., Hetsroni, G., 2000. Thermohydrodynamic characteristics of two-phase flow in a heated capillary. Int. J. Multiphase Flow 26, 1063–1093.

Peles, Y.P., Yarin, L.P., Hetsrohi, G., 2001. Steady and unsteady flow in a heated capillary. Int. J. Multiphase Flow 27, 577–598.

Peng, X.F., Wang, B.X., 1993. Forced convection and flow boiling heat transfer for liquid flowing through microchannels. Int. J. Heat Mass Transf. 36, 3421–3427.

Peng, X.F., Wang, B.X., 1994. Cooling characteristics with microchanneled structures. J. Enhanc. Heat Transf. 1, 315–326.

Peng, X.F., Wang, B.X., 1998. Forced-convection and boiling characteristics in microchannels Heat Transfer Proceeding of the 11th IHTC 1, Kuongju, Korea, pp. 23–28.

Peng, X.F., Wang, B.X., Peterson, G.P., Ma, H.B., 1994. Experimental investigation of heat transfer on flat plates with rectangular microchannels. Int. J. Heat Mass Transf. 37, 127–137.

Peng, X.F., Peterson, G.P., Wang, B.X., 1996. Flow boiling in binary mixtures in microchannels plates. Int. J. Heat Mass Transf. 39, 1257–1263.

Peng, X.F., Hu, H.Y., Wang, B.X., 1998. Boiling nucleation during liquid flow in microchannels. Int. J. Heat Mass Transf. 41, 101–106.

Peterson, G.P., Ha, J.M., 1998. Capillary performance of evaporating flow in microgrooves: an approximate analytical approach and experimental investigation. Trans. ASME, J. Heat Transf. 120, 743–751.

Reid, R.C., Prausnitz, J.M., Poling, B.E., 1987. The Properties of Gases and Liquids. McGraw-Hill, New York.

Seaver, M., Galloway, A., Manuchia, T.J., 1989. Acoustic levitation in a free-jet wind tunnel. Rev. Sci. Instrum. 60, 3452–3458.

Triplett, K.A., Chiaasiaah, S.M., Abdel-Khalik, S.I., Sadowski, J.L., 1999. Gas–liquid two-phase flow in microchannels. Part 1: two-phase flow patterns. Int. J. Multiphase Flow 25, 377–394.

Triplett, K.A., Chiaasiaah, S.M., Abdel-Khalik, S.I., LeMouel, A., McCord, B.N., 1999. Gas–liquid two-phase flow in microchannels. Part 11: void fraction and pressure drop. Int. J. Multiphase Flow 25, 395–410.

Yuan, H., Prosperetti, A., 1999. The pumping effect of growing and collapsing bubbles in a tube. Micromech. Microeng. 9, 402–413.